24th Applied Aerodynamics Conference
5 - 8 June 2006, San Francisco, California

AIAA 2006-3655

Aerodynamics of Wedge-Shaped Deflectors for Jet Noise Reduction

Dimitri Papamoschou*, An Vu†, and Andrew Johnson‡.
University of California, Irvine, CA, 92697-3975

A wedge-shaped deflector placed in the fan exhaust of a turbofan engine can reduce jet noise in a range of azimuthal directions opposite the wedge. The aerodynamics of the fan flow deflector (FFD) wedge are investigated with pressure surveys and flow visualization. The flow field is found to differ substantially from that of a classical wedge-shaped cylinder. There is a significant force developed on the side of the FFD wedge, whereas the classical wedge develops nearly zero side force. The base pressure coefficient of the FFD wedge is substantially less negative than that of the classical wedge. Consequently, the FFD wedge develops about 75% less drag than one would have expected from 2D wedge data.

Nomenclature

c	=	wedge chord length
C_D	=	sectional drag coefficient
C_L	=	sectional lift (sideforce) coefficient
C_P	=	pressure coefficient
h	=	wedge height
M	=	Mach numbers
NPR	=	nozzle pressure ratio=p_0/p_a
p	=	pressure
u,v,w	=	velocity components
U	=	free stream velocity
V	=	velocity magnitude = $(u^2+v^2+w^2)^{1/2}$
x,y,z	=	Cartesian coordinates
α	=	wedge half angle
γ	=	specific heat ratio
ρ	=	density

Subscripts

0	=	total (stagnation)
∞	=	free stream (nozzle exit)
b	=	wedge base

I. Introduction

Suppression of noise from engines of jet aircraft is one of the most topical and challenging problems of modern aeronautics. One of the most intractable sources of noise is jet mixing noise, namely the sound generated from turbulent mixing of the jet plume with the ambient air. To date, the vast majority of methods to suppress jet mixing noise have centered on mixing enhancement. Recently, a new approach for jet noise reduction of turbofan engines was developed in the UCI Jet Aeroacoustics Lab[1]. It involves deflection of the fan stream downward relative to the core stream. The misalignment of the two streams creates a thick low-speed layer on the underside of the jet, which reduces velocity gradients and hence sound emitted in the direction of the ground. The fan flow deflection (FFD) is

* Professor, Department of Mechanical and Aerospace Engineering, 4200 Engineering Gateway, Irvine, CA 92697-3975, AIAA Associate Fellow.
† Undergraduate Researcher, Department of Mechanical and Aerospace Engineering, 4200 Engineering Gateway, Irvine, CA 92697-3975, AIAA Student Member.
‡ Graduate Researcher, Department of Mechanical and Aerospace Engineering, 4200 Engineering Gateway, Irvine, CA 92697-3975, AIAA Student Member.

achievable with aerodynamic surfaces inserted in the fan stream that turn the fan stream in the desired direction while maintaining a coaxial nozzle exit. The technique has been studied experimentally in coaxial nozzles with conventional[1] and realistic geometries[2].

One class of FFD devices are airfoil-shaped vanes internal to the fan duct. The aerodynamics of such vanes were recently investigated computationally[3]. Lift and drag coefficients were found to be in line with those of an external airfoil subjected to flow conditions inside the fan duct. Another, more intriguing type of deflector is a wedge placed at the exit of the fan duct, as shown in Fig.1. The wedge, in consort with the flow lines of the nozzle[4,5], deflects the fan flow downward and in the sideline direction. A representative mean velocity profile is shown in Fig. 2. Figure 3 plots sample noise reductions. The wedge is envisioned as an actuated device, deployed when noise reduction is needed and stowed otherwise.

A question that naturally arises is: what are the aerodynamic penalties of a wedge-shaped surface placed in the exhaust of the fan stream. The classical two-dimensional wedge is known to have significant drag owing to the large suction on its base. However, the FFD wedge experiences different boundary conditions from the classical wedge. On the top side of the FFD wedge, we have a free surface with pressure equal to the ambient pressure. The base of the wedge is in communication with the ambient pressure, so its pressure is not expected to be much below ambient. More generally, it is desired to know the flow characteristics of the wedge in order to optimize its shape for noise reduction and reduce penalties to the minimum possible.

Because the UCI aeroacoustics experiments are of very small scale (about 1/50th scale of a full engine), the wedge dimensions are on the orders of millimeters, which makes instrumentation of the wedge very challenging. For this reason, a scaled-up experiment was envisioned specifically for studying the wedge aerodynamics. It used an existing high-aspect ratio rectangular nozzle to simulate the flow over a portion of the fan annulus. This paper describes preliminary flow visualization and pressure data that illuminate the aerodynamics of the FFD wedge and provide estimates of its aerodynamic coefficients.

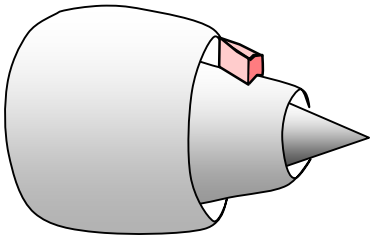

Fig.1 Configuration of wedge-shaped fan flow deflector.

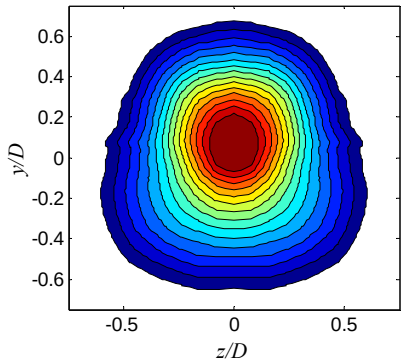

Fig.2 Distortion of mean velocity profile at an axial station near the end of the primary potential core. Noise reduction occurs in the downward (y<0) and sideward directions. From Ref. 5.

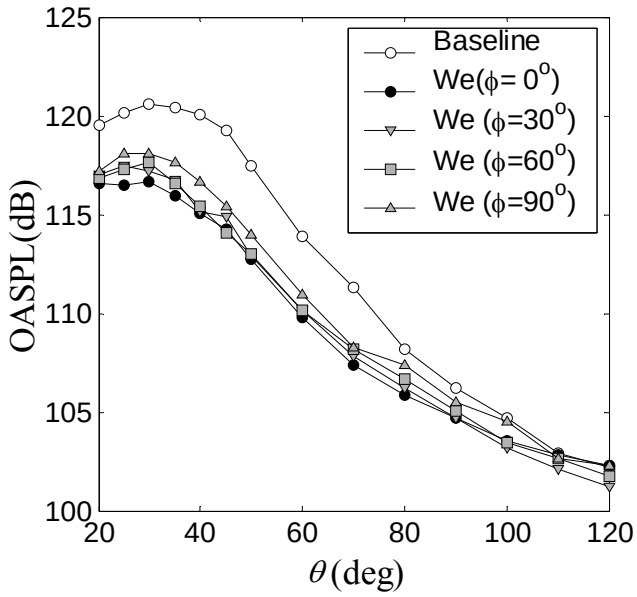

Fig.3 Overall sound pressure level versus polar angle (relative to jet axis) for a variety of azimuth angles ϕ (ϕ=0º denotes the downward vertical.) "Baseline" is the clean nozzle and "W_e" is the case with the external wedge. From Ref. 2.

II. Experimental Setup

The experiments utilized an existing high-aspect ratio rectangular nozzle apparatus regularly used for the study of supersonic nozzle flow separation. A full description of the facility can be found in Ref. 6. The nozzle has flexible walls and can assume convergent-divergent, convergent, or straight shapes. In this instance, the nozzle walls were straight, terminating in an exit height of 18 mm and width of 51 mm.

A wedge with 30° full angle (half angle α=15°) was fabricated from aluminum. Its chord length was c=49 mm, and its height was h=28 mm. The wedge was mounted on a wall surface aligned with the bottom wall of the nozzle. The wedge apex was situated 5.3 mm from the nozzle exit. The setup is shown in Fig. 4. One axial row and four transverse columns (three on the side and one on the base) of static pressure ports were drilled, as depicted in Fig. 5. Each static pressure port had a diameter of 0.8 mm. The axial row contained 16 ports, 12 on the side and 4 on the base. The port closest to the wedge apex was situated at x/c=0.13. Each transverse column contained 5 equally spaced ports, from y/h=0.091 to 0.818. The axial and transverse ports were alternatively connected to a Scanivalve system. The nozzle pressure ratio (NPR) varied from 1.2 to 2.0 in increments of 0.2. Correspondingly, the nozzle exit velocity varied from 170 m/s to 325 m/s, and the Reynolds number (based on chord length) varied from 0.6×10^6 to 1.4×10^6. For each NPR, several axial and transverse pressure surveys were conducted. Figure 6 presents the nomenclature for lift (sideforce) and drag. In interpreting these measurements, it helps to consider the wedge as consisting of two symmetric halves; we are interested in the forces acting on each half.

In addition to pressure measurements, rudimentary flow visualization was done by applying drops of ink on the wedge surface and photographing the resulting streaklines with the flow turned on.

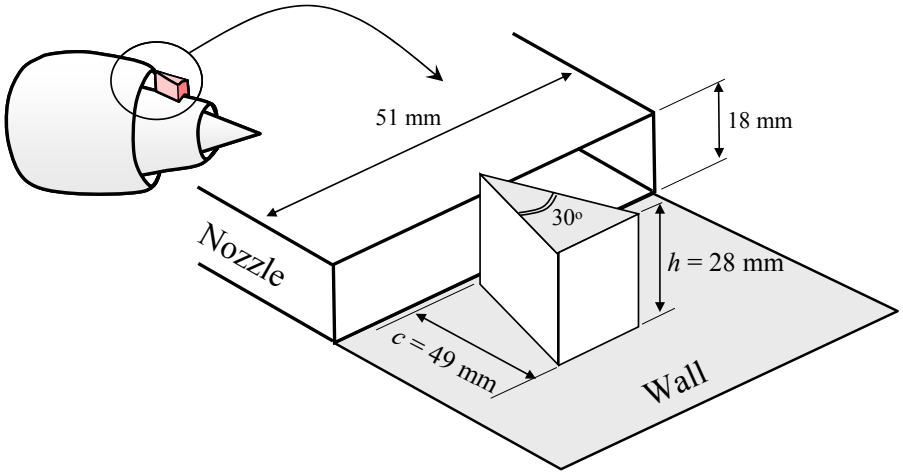

Fig.4 Experimental setup for investigation of wedge flow.

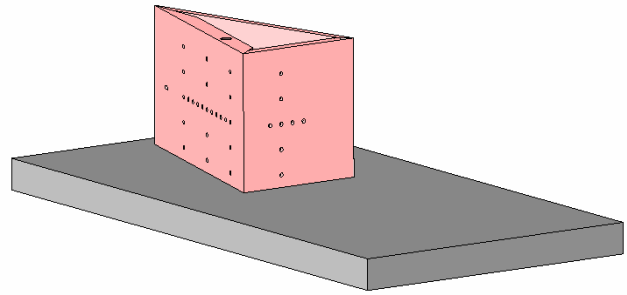

Fig.5 CAD drawing of wedge showing locations of static pressure ports.

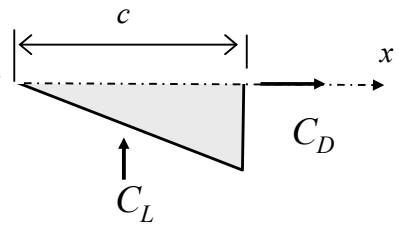

Fig.6 Illustration of lift (sideforce) coefficient C_L and drag coefficient C_D acting on the half-wedge.

III. Results

A. Flow Visualization

Figure 7 shows streaklines on the wedge surface at NPR=2.0. The appearance of streaklines at other NPRs is similar. Even though the visualization method is crude, it helps bring out some very important features of the wedge flow. We observe that flow near the apex in the vicinity of the free surface is tilted nearly vertically. The streaklines at the bottom of the wedge are horizontal, a consequence of the wall boundary condition. The behavior at the free surface can be understood by considering that, on the free surface, the velocity magnitude must remain constant and equal to the value of the freestream (nozzle-exit velocity)

$$V^2 = u^2 + v^2 + w^2 = U_\infty^2$$

Symmetry of the flow at the apex imposes that $u = w = 0$. This means that $v = U_\infty$ on the free surface at the apex, which explains the vertical motion seen on the picture. A cartoon of the streamline pattern is offered in Fig.8. There is only one stagnation point, at the apex on the bottom of the wedge. The streamline from the stagnation point is aligned with the wall. As we move away from the wall, the streamlines tilt increasingly upward. As the streamlines detach from the top of the wedge they probably form a vortical pattern, although further flow visualization is needed to confirm this.

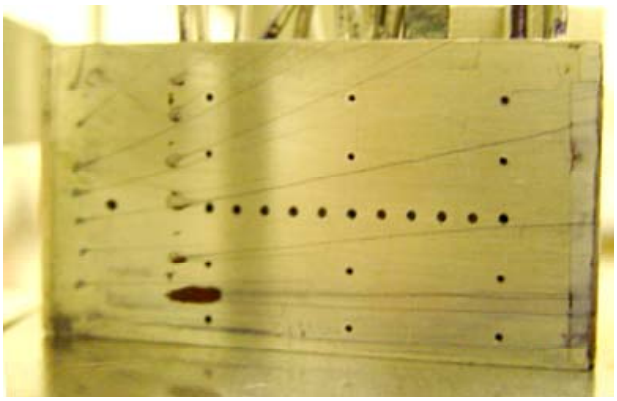

Fig.7 Surface flow visualization of streaklines on wedge surface. NPR=2.0

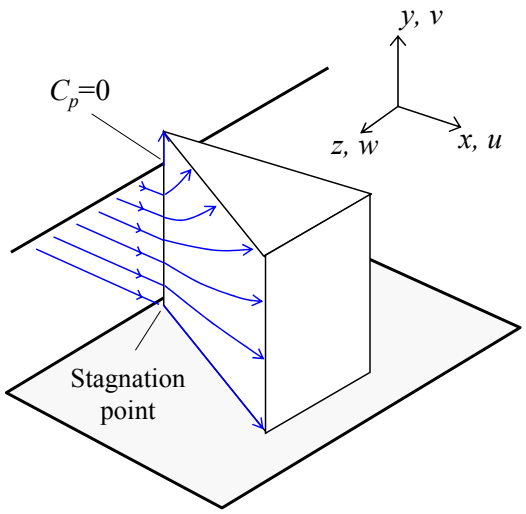

Fig.8 Cartoon of streamline pattern around wedge.

B. Static pressure surveys

The pressure collected at the static pressure ports is presented in terms of the pressure coefficient

$$C_P = \frac{p - p_\infty}{\frac{1}{2}\rho_\infty U_\infty^2} = \frac{2}{\gamma M_\infty^2}\left(\frac{p}{p_\infty} - 1\right) \tag{1}$$

Figure 9 plots the axial distribution of C_P, measured on the row of static pressure ports shown in Fig.5, for NPR=1.2, 1.6, and 2.0. The normalized coordinate x/c is used in plotting the data. For all NPRs, C_P is positive on the side of the wedge and negative on the base. It decreases rapidly with axial distance near the wedge apex and more gradually downstream. As NPR increases, the distribution of C_P on the side of the wedge becomes flatter. The base pressure coefficient is -0.20 for NPR=1.2 and increases to -0.16 for NPR=2.0. There is no significant variation of pressure along the row of ports on the base of the wedge.

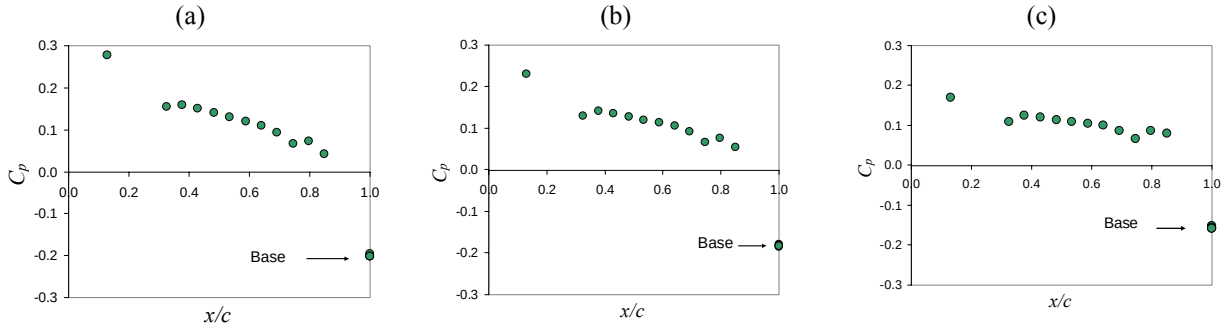

Fig. 9 Axial distributions of pressure coefficient at y/h=0.455. (a) NPR=1.2; (b) NPR=1.6; (c) NPR=2.0

It is instructive to compare the axial C_P distributions of the FFD wedge with those of a classical 2D wedge (a triangular cylinder) having the same angle. Tanner[7] investigated, theoretically and experimentally, the incompressible flow field and pressure distribution for 2D wedges of various angles. His C_P distribution on a wedge with α=15° is compared to the FFD wedge distribution in Fig.10. There is a dramatic difference between the two

distributions. In the classical case, the wedge develops compression over the fore portion of the side and strong suction over the aft portion of the side; in contrast, the side of the FFD wedge has compression throughout. The base pressure coefficient for the classical wedge is C_{Pb}=-1.0 while it is -0.2 for the FFD wedge. This indicates that the FFD wedge develops much less drag than the classical wedge. The moderate negative C_{Pb} of the FFD wedge is a consequence of the exposure of the wedge base to the ambient pressure.

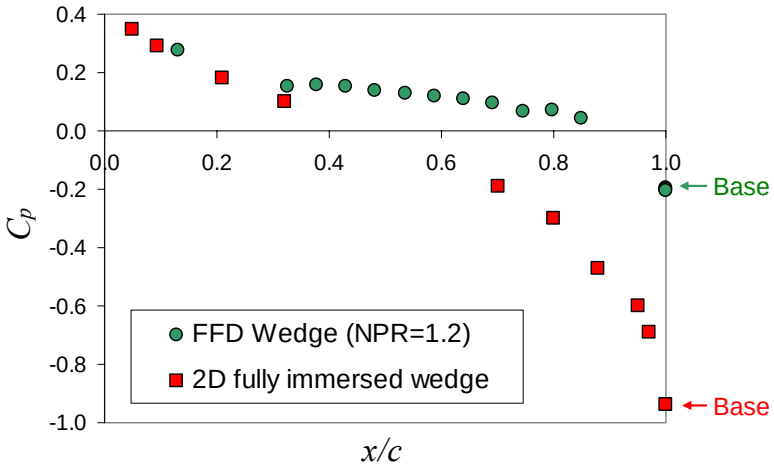

Fig. 10 Comparison of Cp-distribution with classical two dimensional wedge (Ref.7).

To get a fuller picture of the pressure distribution on the FFD wedge, we examine the transverse distributions of C_P on the four columns of ports shown in Fig.5. Figure 11 plots C_P versus y/h for the four locations of the columns (three on the side and one on the base) and for NPR=1.2, 1.6, and 2.0. On the side of the wedge, the transverse distributions of C_P are fairly flat and tend to zero as we approach the top of the wedge. They do not quite reach zero at the top because the flow deflects upward, as shown in Figs 7 and 8, so there is significant flow velocity even at the top pressure ports. For NPR=2.0, the distribution near the trailing edge of the side of the wedge develops a significant bump at the mid-height of the wedge, which is not presently understood. On the base of the wedge, C_P drops and then rises with transverse distance. The minimum value occurs roughly where the axial survey of C_P was conducted (y/h=0.455).

Linear interpolation of the axial and transverse pressure measurements allows a preliminary matrix of the C_P values over the side surface of the wedge. Resulting contour maps are shown in Fig. 12 for NPR=1.2, 1.6, and 2.0. Near the wedge apex, the variation of C_P from large positive value near the wall to near-zero on the free surface is evident. The contours reflect to some extent the upward motion of the streamlines noted in the flow visualization of Fig. 7. While there are no significant differences in the contours at NPR=1.2 and 1.6, for NPR=2.0 (supersonic fully-expanded flow) the contours become peaky near the mid-height of the wedge, as reflected in the corresponding transverse distributions of Fig. 11.

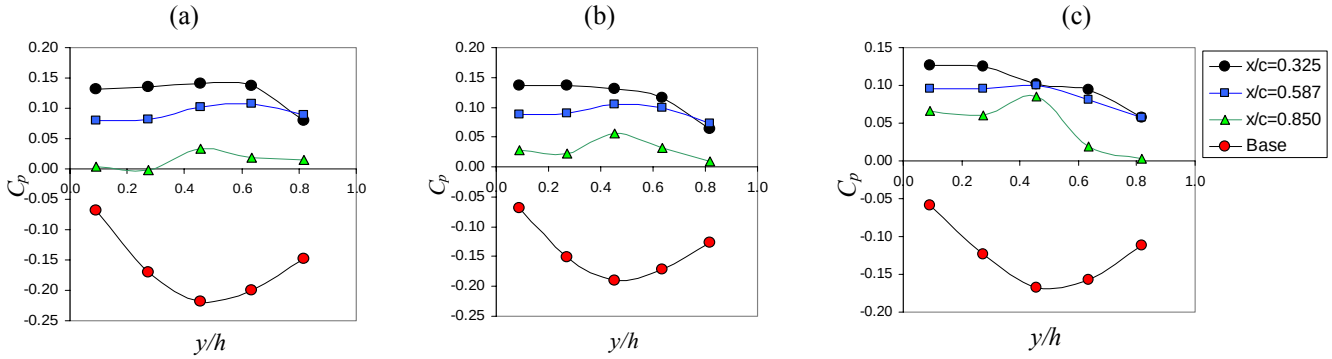

Fig. 11 Transverse distributions of pressure coefficient at three axial positions along side of wedge and at wedge base. (a) NPR=1.2; (b) NPR=1.6; (c) NPR=2.0.

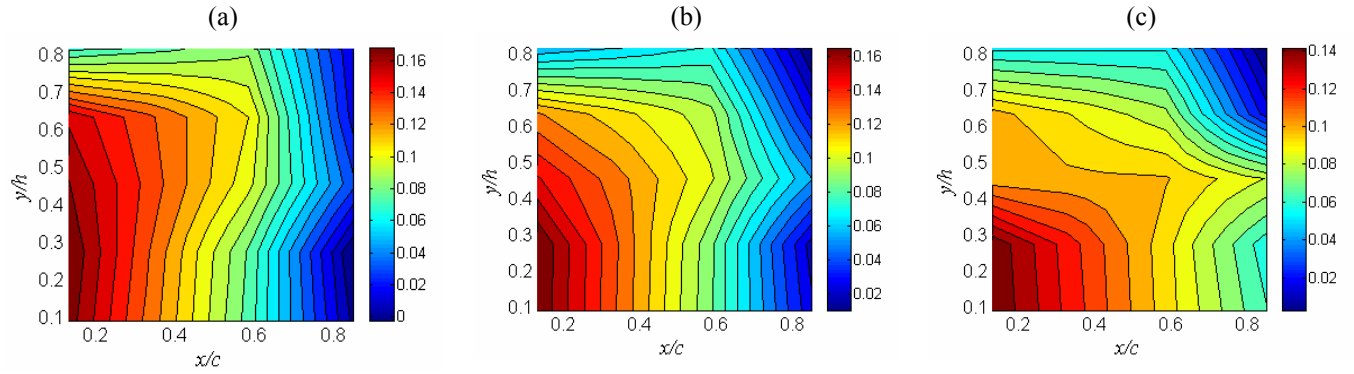

Fig. 12 Contour maps of pressure coefficient over measured area on the side of the wedge. (a) NPR=1.2; (b) NPR=1.6; (c) NPR=2.0.

C. Calculation of Aerodynamic Coefficients

Given the C_P distribution on the surface of the wedge, calculation of the sectional lift (sideforce) and drag coefficients is straight forward:

$$C_L = \int_0^1 C_P d(x/c) \tag{2}$$

$$C_D = (C_L - C_{Pb}) \tan\alpha \tag{3}$$

Integration for C_L includes only the side of the wedge (not the base). A problem with the existing data is that the pressures at the apex and trailing-edge corner of the wedge were not measured, due to the impracticality of locating pressure ports at those points. The value of C_P at the trailing edge was assumed equal to the value at the base to satisfy pressure balance of the free surface detaching from the corner. This choice has very little impact on the computation of the aerodynamic coefficients. Treatment of the apex is more complicated. As discussed earlier, symmetry of the flow at the apex requires that the axial and transverse velocity components be zero (u=v=0). On the wall (y=0), the spanwise velocity is also zero (w=0), therefore the apex on the wall is a stagnation point. The pressure coefficient at the stagnation point is

$$C_{P0} = \frac{2}{\gamma M_\infty^2}\left(\frac{p_0}{p_\infty} - 1\right) = \frac{2}{\gamma M_\infty^2}\left(\text{NPR} - 1\right) \tag{4}$$

It approaches the value of 1 as $M_\infty \rightarrow 0$. As noted in the flow visualization section, the pressure at the apex above the height of the nozzle (y/h>0.64) equals the ambient pressure (C_P=0). Therefore, as we move along the apex from the wall to the top of the wedge, C_P drops from C_{P0} at y/h=0 to 0 for $y/h \geq 0.64$. Here we assume a linear decay

$$C_{P,apex} = \begin{cases} C_{P0}\left(1 - \dfrac{y/h}{0.64}\right), & y/h < 0.64 \\ 0, & y/h \geq 0.64 \end{cases} \tag{5}$$

Another critical aspect is the axial transition of C_P from the apex to the first measurement point. The shape of this transition has moderate influence on the calculation of the aerodynamic coefficients. Here we invoke the result of incompressible potential theory for flow around a wedge. In the vicinity of the apex of the wedge, we have

$$V(x) = kx^{\beta/(2-\beta)}, \quad \beta = 2\alpha/\pi \tag{6}$$

where x is supposed to be the coordinate along the side of the wedge but, with proper treatment of the constant k, becomes the axial coordinate. In our case, α=15° and thus β=1/6, yielding

$$V(x) = kx^{0.091}$$

Using once again incompressible relations,

$$C_P = 1 - \left(\frac{V}{U_\infty}\right)^2 = 1 - K\left(\frac{x}{c}\right)^{0.182}$$

where various constants were absorbed into the new constant K. Now we generalize this relation to the compressible case of the wedge,

$$C_P = C_{P,apex} - K\left(\frac{x}{c}\right)^{0.182} \tag{7}$$

The constant K is determined from the first experimental value of C_P in the axial direction. Equation 7 is an approximation of the axial distribution of C_P near the wedge apex for a given transverse plane. Figure 13 presents examples of such distributions and their blending with the experimental data at stations downstream of the apex. Integration of those curves allows estimates of C_L and C_D per Eqs. 2 and 3.

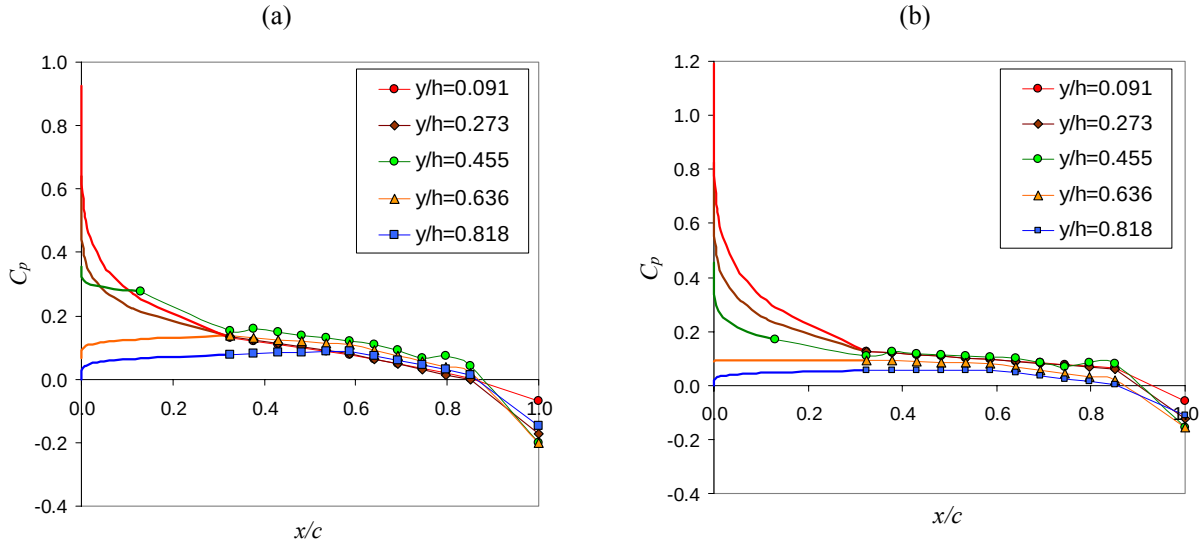

Fig. 13 Axial distributions of pressure coefficient including extrapolation to wedge apex. (a) NPR=1.2; (b) NPR=2.0.

Figure 14 plots the resulting distributions of sectional C_L and C_D for the transverse planes investigated and for three NPRs. The sectional C_L decreases monotonically with transverse distance, while the sectional C_D first rises and then drops with transverse distance. Both coefficients tend to zero as y/h approaches 1. As NPR increases, the value of C_L near the wall ($y/h \rightarrow 0$) tends to increase. There is no significant change in the C_D distribution with increasing NPR.

By taking the average value of each the transverse distribution we arrive at estimates of the overall lift and drag coefficients. They are listed in Table 1, together with the "aerodynamic efficiency" parameter C_L/C_D. Compared to an airfoil at the same angle of attack, the wedge is a much weaker (about 10 times less) generator of lift. The lift-to-drag ratio starts at 1.5 at low NPR and increases to 1.8 at high NPR.

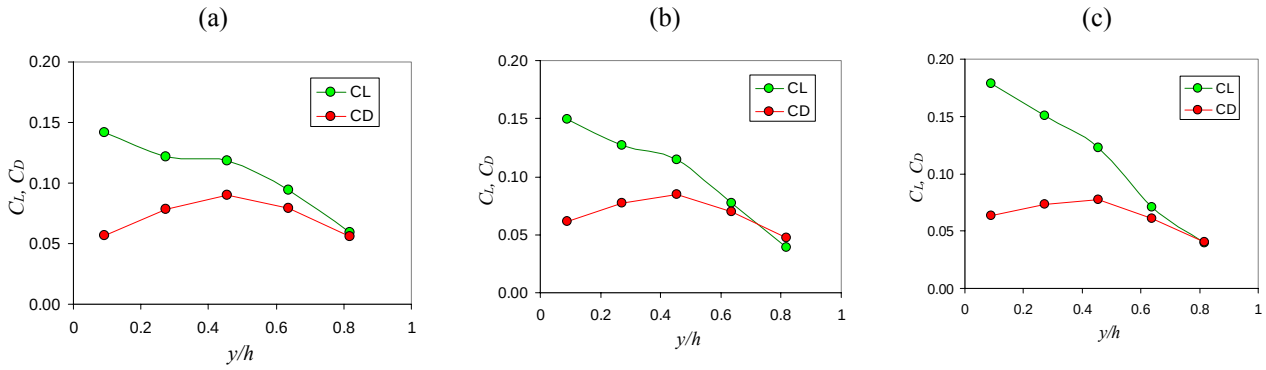

Fig. 14 Transverse variation of sectional lift and drag coefficients. (a) NPR=1.2; (b) NPR=1.6; (c) NPR=2.0

It is interesting to compare our data with the results of the classical 2D wedge studied by Tanner[7] (Fig.10). Integration of Tanner's C_P yields a lift coefficient of practically zero and a drag coefficient of 0.25. The fan flow deflector wedges therefore have a drag coefficient about 75% less than that of a fully-immersed two-dimensional wedge.

Table 1. Total Aerodynamic Coefficients

FFD Wedge	NPR	C_L	C_D	C_L / C_D
	1.2	0.105	0.071	1.49
	1.4	0.108	0.071	1.52
	1.6	0.109	0.067	1.62
	1.8	0.107	0.063	1.69
	2.0	0.110	0.063	1.75
2D Fully Immersed wedge (Ref.7)	1.0*	-0.001	0.252	0.00

* Incompressible

D. Impact on Engine Thrust

Accurate prediction of engine thrust loss requires elaborate computations and validation by large-scale thrust measurements. This is outside the scope of the present work. Here we use the drag coefficient data from our measurements to come up with a very rough, order-of-magnitude estimate of the thrust loss caused by the FFD wedge in a high-bypass turbofan engine. We consider a wedge with 15° half angle and dimensions (relative to the nozzle size) typical of those used in the aeroacoustics experiments[2].

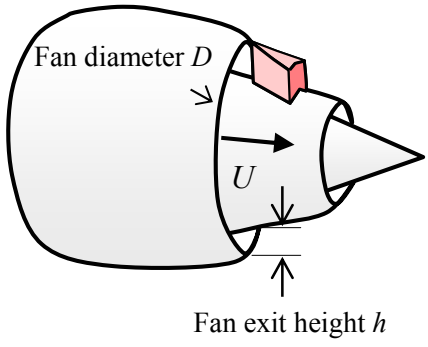

Fig. 15 Key parameters for fan stream of turbofan engine.

Figure 15 presents the key parameters for this simple calculation. Treating the exit of the fan nozzle as a thin annulus of height h and diameter D, and assuming pressure-matched flow, the static thrust of the fan stream is

$$F = \rho U^2 \pi D h \tag{8}$$

Assuming that the height of the wedge is equal to the height of the fan nozzle, the drag of the wedge is

$$D = 2C_D \frac{1}{2} \rho U^2 hc \tag{9}$$

The factor of 2 in front of C_D accounts for the fact that a full wedge consists of two half wedges; recall that our definitions of C_D and C_L are based on the half-wedge. Dividing Eq.9 by Eq.8,

$$\frac{D}{F} = \frac{1}{\pi} C_D \frac{h}{D} \frac{c}{h} \tag{10}$$

Examining the designs of turbofan engines with bypass ratios 5-8 (see for example Ref.2), one finds that h/D~0.1. Wedges tested at UCI had chord lengths about three times their height, c/h~3. Inserting these numbers in Eq.10,

$$\frac{D}{F} \sim 0.1 \, C_D \tag{11}$$

At takeoff conditions, the NPR for the fan exhaust in the range of 1.6-2.0. For the average drag coefficient in that range (Table 1),

$$\frac{D}{F} \sim 0.006$$

In other words, the thrust loss for the fan stream is around 0.6%. For an engine with bypass ratio 5, the fan stream provides about 70% of the total thrust. The thrust loss for the entire engine is thus estimated at 0.4%. It is emphasized that these are very rough numbers based on a simplified analysis. Their purpose is to provide an overall sense as to what aerodynamic penalty might be expected. Recall that the wedge is envisioned as an actuated device, so this penalty would be incurred only during the noise-sensitive portions of flight. Optimization of the wedge shape could lead to configurations with less drag and better flow deflection patterns.

IV. Conclusions

The aerodynamics of the fan flow deflector (FFD) wedge with 15° half angle were investigated in a facility that enabled pressure instrumentation of the wedge and preliminary flow visualization. A fairly complex flow field emerged, with a free surface tilting upward and resulting divergent streamlines on the side of the wedge. There are substantial differences with the classical problem of a 2D wedge. The FFD wedge develops a significant force on its side, whereas the classical wedge develops nearly zero side force. The base pressure coefficient of the FFD wedge is substantially less negative than that of the classical wedge. Consequently, the FFD wedge develops about one quarter of the drag one would have expected from 2D wedge data. The sideforce-to-drag ratio of the FFD wedge ranges from 1.5 at moderate subsonic freestream Mach number to 1.8 at near-sonic Mach number. The static-thrust loss on a high-bypass engine caused by this type of wedge is estimated at around 0.5%.

Acknowledgments

The support by NASA Glenn Research Center is gratefully acknowledged (Grant NAG-3-2345 monitored by Dr. Khairul B. Zaman and Dr. James Bridges.) The method and system of noise suppression via deflection of the bypass and/or core streams is proprietary to the University of California. U.S. Patent Pending.

References

[1]Papamoschou, D., "New Method for Jet Noise Suppression in Turbofan Engines," AIAA Journal, Vol. 42, No.11, 2004, pp. 2245-2253.

[2]Papamoschou, D. and Nishi, K.A., "Jet Noise Suppression with Fan Flow Deflectors in Realistic-Shaped Nozzle," AIAA Paper 2005-0993, Jan. 2005; to appear in the *AIAA Journal*.

[3]Murayama, T., Papamoschou, D., and Liu, F. "Aerodynamics of Fan Flow Deflectors for Jet Noise Suppression," AIAA Paper 2005-0994, Jan. 2005.

[4]Zaman, K.B.M.Q. and Papamoschou, D. "Effect of a Wedge on Coannular Jet Noise", AIAA Paper 2006-0007, Jan. 2006.

[5]Papamoschou, D. and Shupe, R.S.., "Effect of Nozzle Geometry on Jet Noise Reduction Using Fan Flow Deflectors," AIAA Paper 2006-2707, May 2006.

[6]Papamoschou, D. and Zill, A., "Fundamental Investigation of Supersonic Nozzle Flow Separation," AIAA Paper 2004-1111, Jan. 2004.

[7]Tanner, M. "Determination of base drag with application to the near wake of wedges," Mitteilungen aus dem Max-Planck Institut für Strömungsforschung und der Aerodynamischen Versuchsanstalt, Nr. 31, Göttingen, 1964.